Chemical Engineering Science 191 (2018) 78–86

Contents lists available at ScienceDirect

Chemical Engineering Science

journal homepage: www.elsevier.com/locate/ces

Movement of a liquid droplet within a fibrous layer: Direct pore-scale modeling and experimental observations

H. Aslannejad [a,*], H. Fathi [b], S.M. Hassanizadeh [a], A. Raoof [a], N. Tomozeiu [c]

[a] Department of Earth Sciences, Utrecht University, Utrecht, The Netherlands
[b] Department of Mechanical Engineering, Shahid Bahonar University of Kerman, Kerman, Iran
[c] Research & Development, Océ Technologies B.V., Venlo, The Netherlands

HIGHLIGHTS

- Spreading and penetration of a droplet on paper were simulated using a pore-scale model.
- The effect of change in contact angle and ink physical properties were studied.
- Contact angle of zero showed largest penetration and no moving away from jet location.
- Ink-like liquid moved slower than water droplet and its penetration depth was smaller.

ARTICLE INFO

Article history:
Received 12 March 2018
Received in revised form 7 June 2018
Accepted 22 June 2018
Available online 27 June 2018

Keywords:
Inkjet printing
Fibrous porous medium
Paper
Pore-scale simulation
Ink spreading/penetration

ABSTRACT

In this study, the spreading of a liquid droplet on the surface of a fibrous paper and its penetration into the paper is studied. The spreading of the droplet was visualized using confocal microscopy and the penetration depth was quantified using Automatic Scanning Absorptiometry (ASA) measurements. The three-dimensional structure of the paper was obtained through micro-tomography imaging with a resolution of 0.9 μm. The obtained images were used to reconstruct the pore space, which was in turn used in direct numerical simulations of penetration of a droplet into paper. Simulations were performed using open source code OpenFOAM, which solves equations of two-phase flow (in our case air and water) in pores based on the Volume of Fluid Method. Simulation results showed a good agreement with the experimental observations. In particular, the dimensions of spreading area of a droplet and the depth of penetration were simulated reasonably well. Then, we used the model to investigate effects of changes in various liquid properties on spreading and penetration of a droplet liquid. We made calculations for three different values of contact angle (*CA*): 0°, 60°, and 120°. We found the largest penetration depth for *CA* = 0. For *CA* = 60 and *CA* = 120, we found that the liquid droplet moved sideways from the jetted location, which is not favorable in inkjet printing. We also made simulations with larger values for viscosity and density, based on properties of an ink-based liquid used in inkjet printing. The results have shown a slower spreading and penetration compared with water. The model can be used to study effects of changes in either ink physical properties or paper layer microstructure on final spreading/penetration extent.

1. Introduction

Cellulose fibers are renewable natural materials, which are encountered in many industrial applications, such as paper and printing, packaging, and paper-based diagnostic devices. Their main features important to these applications are light weight, mechanical strength, and low cost (Podsiadlo et al., 2005).

In the majority of applications, a fibrous layer comes into contact with some liquid (mainly water-based liquid). Because cellulose fibers are hydrophilic, liquid will move rapidly along and into fibers. This can cause unwanted spreading of ink in paper, for example in case of inkjet printing (Fig. 1), or swelling of fibers, which can be a problem in the case of packaging application.

Generally, a fibrous layer can be considered as a porous medium, although liquid flow in the layer is different from traditional porous media. Usually, a liquid moves into pores of a porous network and, based on connectivity of pores, invades some of them. However, in the case of a fibrous layer, water moves first on the

* Corresponding author at: Environmental Hydrogeology Group, Universiteit Utrecht, Princetonplein 9, 3584 CC Utrecht, The Netherlands.
E-mail address: H.aslannejad@uu.nl (H. Aslannejad).

https://doi.org/10.1016/j.ces.2018.06.054
0009-2509/

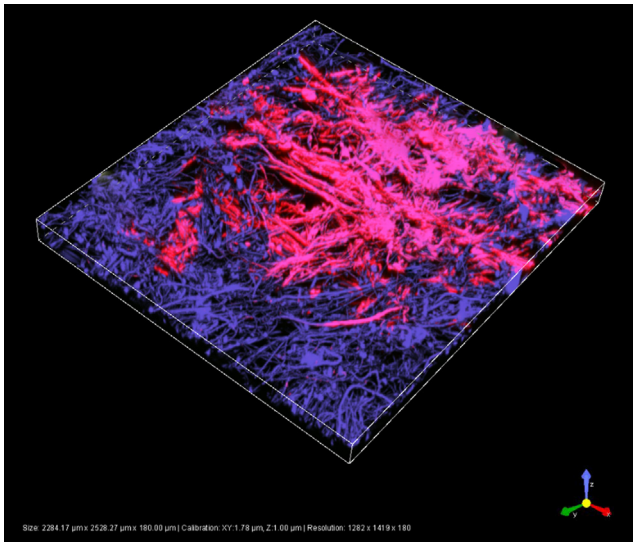

Fig. 1. Water spreading in a fibrous layer; fibers are shown in blue and water in pink. The image was obtained using confocal microscopy.

surface of fibers and/or into them, and then later on fills the pores between fibers (Aslannejad and Hassanizadeh, 2017). Schoelkopf et al. (2000) stated that under a condition of constant wettability and surface energy, pore diameter and geometry are the controlling factors. Therefore, contradictory to Lucas-Washburn equation which predicts the large pores to be filled faster than small pores, liquid droplet in a paper layer proceeds by filling finer pores together with inertial retardation of larger pores and then, viscosity-controlled absorption dynamics becomes prominent. Liu et al. (2017) also considered the difference between coated and uncoated paper from droplet wicking point of view and they conclude that, in case of uncoated paper, the wicking behavior follows neither viscosity-controlled model of Lucas-Washburn nor inertia-included model of Bosanquet. Modaressi and Garnier (2002) also reported such a flow behavior in a partially hydrophobized fibrous layer. They did an experiment and reported that the droplet first imbibed into the fibrous layer forming a pattern in the layer and then when it reached steady state, it was absorbed into the fibers.

In case of inkjet printing, there are two types of paper: plain and coated. Plain papers, made of cellulose fibers, may absorb too much ink. In order to limit ink uptake by plain paper, often a thin layer of coating material is applied on the surface of fibrous layer. However, due to their overall low cost, uncoated papers are more commonly used in inkjet printers. Then, various measures are taken to reduce the uptake of ink and its spreading into the fibrous layer. These relate to the modification of the properties of ink and/or fibers. Effects of such measures have been studied in recent decades. Yarin (2006) studied normal impact of a droplet on dry paper surface and characterized effects of surface roughness, surface texture, and wettability. Modification of liquid properties by adding a polymer mixture was also studied. Xu et al. (2005) reported that by controlling the pressure artificially generated in a gas atmosphere (helium, air, krypton, and SF) during droplet impact on the solid surface, they could control splash of droplet.

Alam et al. (2007) studied the kinetic-energy-driven phase of spreading of a liquid on irregular surface of a porous material using the Volume of Fluid method (VOF). They performed computations and showed that the spreading width is inversely correlated with the depth of penetration. They studied different surface roughness types: flat, randomly located monodisperse hemispheres, and pyramidal structures. Analysis of various roughness parameters and their impact on spreading were done in their work.

Hyväluoma et al. (2006) studied penetration of a liquid in paperboard using Lattice Boltzmann method. They used reconstructed pore space of a sample imaged by micro tomography. Capillary-driven flow into the domain was simulated and compared with well-known Lucas-Washburn equation results. They concluded that there is a need to study and determine advancing of the liquid front into the paper. They also concluded that water penetration occurs along fibers and much faster in the planar direction than in the perpendicular.

Do-Quang et al. (2011) investigated numerically the impact of ink onto the surface of a paper-like structure; they used a model structure as a fibrous web. They simulated multi-phase flow of air and liquid and they determined the penetration pattern of the droplet in the structure. They also studied the impact of change in wettability on penetration.

To the best of our knowledge, there have been little to no direct comparison of spreading of a liquid on a fibrous layer and the degree of its penetration with numerical simulations. In addition, studies involving a liquid with ink-like properties comparable to ink have been limited.

In this study, we focus on not only spreading of a droplet on a paper surface, but also its penetration into the fibrous layer. The fibrous layer pore and fiber structure were reconstructed using high-resolution micro-tomography images. The resulting digitized layer was then used as input in two-phase simulations of penetration of a droplet into the fibrous layer. Simulation results were then compared with experimental results from confocal microscopy and automatic scanning absorptiometry ASA measurements. The effect of wettability change was studied by specifying different values for contact angles. In addition, the effects of change in fluid properties (density, viscosity and surface tension) on resulting penetration/spreading are reported. The results of this study will contribute to a better understanding of the flow in printing paper. By optimizing properties of the liquid and paper, a cheaper production of high quality prints can be made possible. Moreover, results of this research are relevant to the general understanding of interaction of complex fluids with complicated porous structures.

2. Material and methods

2.1. Paper and liquids

A Ziegler uncoated paper sample (Ziegler paper, Switzerland) was used in this study. Fig. 2 shows an SEM image of the cross section and surface of the paper sample. The fibrous layer of paper is

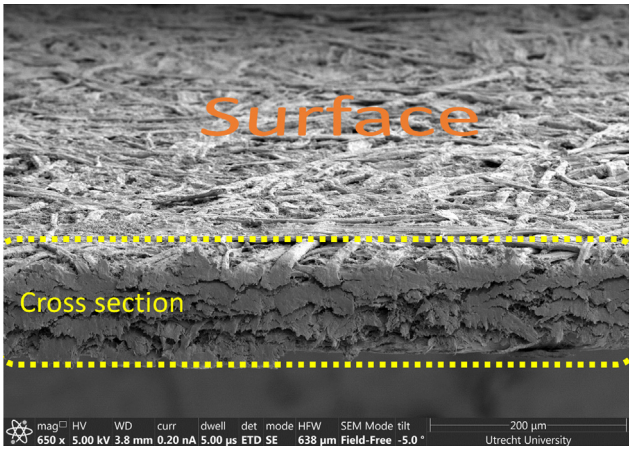

Fig. 2. Three-dimensional SEM image of cross section and surface of a Ziegler paper sample.

an anisotropic medium, where the fibers are aligned with the majority in one direction. In the terminology used in paper fabrication, the major alignment direction is termed the machine direction, and the alignment reflects the flow orientation in the papermaking process. The planar direction perpendicular to this machine running direction is termed the cross-machine direction. The sample had a thickness of 150 μm with mean pore size of 10 μm (Aslannejad and Hassanizadeh, 2017). The porosity of the layer was about 50% and the fiber diameters lay in the range 10–25 μm. In a previous study (Aslannejad and Hassanizadeh, 2017), we determined a permeability value of about 5 Darcy. All paper samples were kept under standard laboratory conditions before imaging and ink pattern visualization.

In experimental observations, water with a very low concentration of fluorescent salt (1 g/l) was used. The salt was added in order to improve tracking and monitoring of water under the confocal microscope. Properties of salt-water were used in simulations of experiments. For a typical inkjet printer, the ink consists of 2–5 wt% dye or pigment, 2–5% surfactants, 30% humectant (ethylene glycol), and 65% water (Lee et al., 2002). In addition to the simulation of our experiments, we also performed numerical modelling of the penetration of an ink-like liquid, having the same properties (namely, viscosity, density, and surface tension) as ink. We did not consider presence of pigments in our simulations.

2.2. Microstructure imaging and reconstruction

An accurate reconstruction of the pore space, with a sufficient resolution, is essential for pore-scale modeling. In order to reconstruct the 3D domain of a fibrous paper sample, imaging was done using micro-computational tomography (μCT), Zeiss Xradia Versa 520, with a resolution of 0.9 μm. A domain of 1000 × 1000 × 150 μm^3 was then reconstructed using watershed segmentation (Aslannejad and Hassanizadeh, 2017). Fig. 3 shows part of the reconstructed fibrous layer with a dimension of 400 × 400 × 150 μm^3.

2.3. Droplet dispenser and confocal microscopy setup

In order to produce a very small ink droplet (comparable with inkjet printer droplets size), a micro droplet dispenser (Microdrop Technologies GmbH, Germany) was mounted next to the microscope objective. The dispenser was able to produce a small droplet with a volume of 180 pL. It was mounted at an angle of 45° to the microscope objective, in order to make it possible shooting the droplet to a location on the paper within the field of view of the confocal microscope (Nikon A1+). Fig. 4 shows the droplet dispenser-microscope setup.

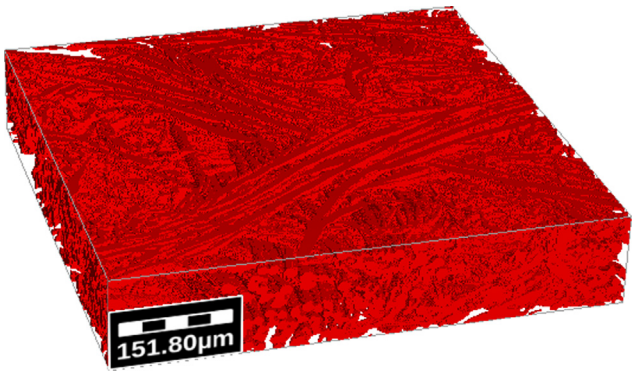

Fig. 3. Reconstructed fibrous layer with dimensions of 400 × 400 × 150 μm.

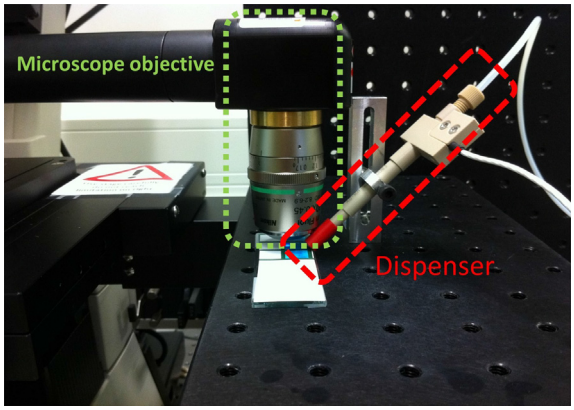

Fig. 4. Droplet dispenser and microscope setup.

Confocal microscopy was used to visualize the liquid distribution in the paper substrate. For visualization, two Argon laser wavelengths were used: 457 nm and 488 nm. Doing so, water and the fibrous layer were clearly distinguishable; fibers and water could be seen in blue and green colors, respectively.

2.4. ASA measurement setup

The Automatic Scanning Absorptiometry (ASA) is an instrument for quantifying uptake of a liquid by paper within a certain time. The ASA instrument we have used (Kumagai Riki Kogyo (KM 500win)) is shown in Fig. 5. The main part of ASA is a horizontal rotary disk (turntable) with eccentric. A piece of paper is placed on the disk and the liquid is delivered onto the paper surface via a nozzle. The nozzle is mounted on an extended arm having a fixed length from a rotation mounting at one end. The mounting has a fixed distance from the axial sample rotation point, like a disk record player. The liquid is delivered from a glass capillary, and the Transferred Liquid Volume (TLV) is monitored within the capillary, and the resultant liquid track on the porous material forms a spiral that can be characterized by its radius and pitch (the distance between the two consecutive radii at the same polar angle).

In a typical analysis of ASA measurements, the penetration depth is estimated from TLV, the nozzle width and length and assuming all pores all filled by the absorbed liquid (Kuijpers et al., 2018). In our experiment, we determined the penetration depth for a given TLV using SEM and observing the cross section of paper.

2.5. Two-phase flow modeling

The spreading of a liquid droplet on the paper surface and its penetration into the fibrous layer was modelled as simultaneous movement of the two phases in interface contact (air and water) in the pore space. Two-phase flow simulations were performed using open source software, OpenFOAM (The OpenFOAM Foundation, 2017. http://www.openfoam.org/ (accessed 22 October 2017)), which solves an extended form of the Navier-Stokes equations. Palakurthi et al. (Palakurthi et al., 2015) verified the solution of OpenFOAM for liquid penetration in virtual fibrous media. They checked the results against Lucas–Washburn kinetics at the microscale, being limited to a parallel bundle of capillaries only, and found them acceptable apart from the very initial stages dominated by inertial forces.

Several studies have employed the Volume of Fluid (VOF method to simulate two-phase flow at the micro- and nanoscale (Fathi et al., 2017). Ability of the VOF method to model micro- and nanoscale processes was shown by Bedram and Moosavi

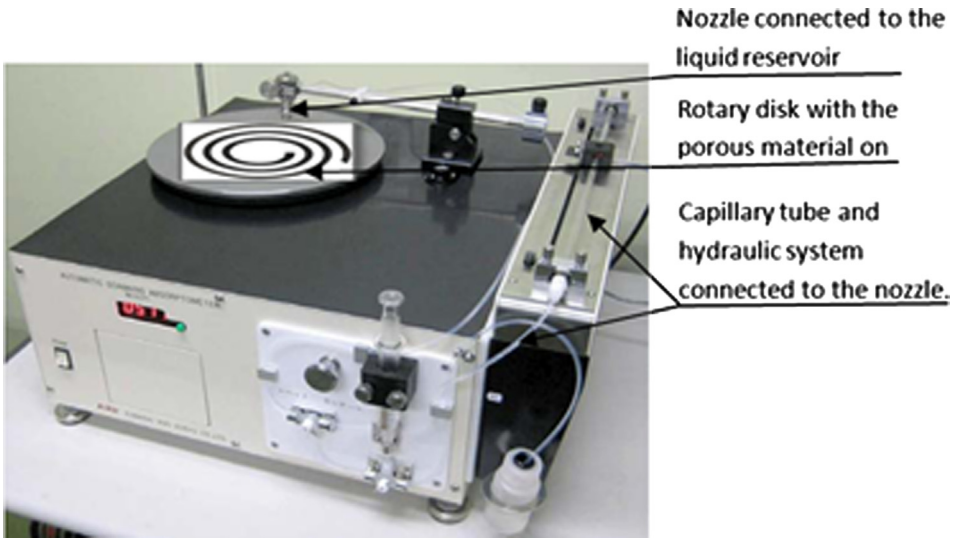

Fig. 5. ASA measurement setup.

(Bedram and Moosavi, 2013). In this method, continuity and momentum balance equations were solved in order to obtain the liquid phase volume fraction in each numerical cell, such that $F_v = \alpha V_{cell}$, where F_v is the volume of liquid phase in a cell with volume V_{cell}. The value of α varies between zero and one. The movement of air-liquid interfaces is simulated by solving a transport equation for α as:

$$\frac{\partial \alpha}{\partial t} + \nabla(U\alpha) + \nabla.(\alpha(1-\alpha)U_r) = 0 \quad (1)$$

in which U_r is the velocity of the interface and defines as:

$$U_r = c_r|U|\frac{\nabla\alpha}{|\nabla\alpha|} \quad (2)$$

The last term of Eq. (1) is non-zero only in cells where an interface exists and α is between zero and one. This term represents a numerical compression term as suggested by Weller (2008) in order to minimize the smearing of the interface. The parameter c_r in Eq. (2) controls the compression of the interface. Following Weller, the value of c_r was taken to be the range $1 \leq c_r \leq 4$ in order to maintain a sharp interface. The physical properties of the "equivalent liquid" in a numerical cell were calculated as averages of properties of the two phase weighted with the volume fraction α. For example, the fluid density at any point within the domain is given by:

$$\rho = \alpha\rho_w + (1-\alpha)\rho_\alpha \quad (3)$$

where ρ_w and ρ_a are the densities of water and air, respectively. The viscosity, μ, is calculated in a similar way. For boundary conditions, we assumed the surface of fibers as solid surfaces with a contact angle of 15 and symmetry condition were applied for the boundaries.

3. Results and discussion

3.1. Experimental results

In order to consider heterogeneity of the fibrous layer and its effect on results, four-different locations on the paper surface were chosen. At each location, a liquid droplet of 180 pL was placed on fibrous layer. The final distributions of water on paper surface, imaged using confocal microscopy, are shown in Fig. 6; fibers are seen in blue color and ink-like liquid in green color. The extent of spreading was measured in two directions, i.e. in the machine direction and cross-machine direction.

The penetration depth was found to be smaller than the spreading extent in planar directions. This is to be expected as the fibers lie mainly in the plane of paper since most fibers are laid down oriented in machine direction. Along the machine direction, the ink spread was in the range of 180–210 μm, while in the perpendicular direction it spread around 140–190 μm.

During the experiment, it was observed that as soon as droplet arrives on surface of layer, it starts to spread on fibers and then evaporation occurs immediately. Although swelling was expected, but due to very small amount of water and relatively fast evaporation at the end of spreading, no change in fiber size was recorded. In the other words, for a single droplet of 180 pL, no fiber swelling was observed, consequently, that can be assumed that in case of single droplet, water intake of fibers is negligible.

The penetration depth for a 200 pL of liquid was determined to be 50 μm, using ASA measurements as explained earlier. Since the major axes of fibers are in the plane of the sheet, the spreading length is larger than the vertical penetration depth.

3.2. Simulation results

Since the sheet is so thin, the traditional penetration model is used, i.e. that of direct porosity-filling, in contrast to the wicking and spread function employing the software modelling based on volume of fluid. For the simulation of experiments, a spherical droplet with diameter of 75 μm was placed on the fibrous layer (Fig. 7) at four different locations. The reconstructed pore geometry was used as the modelling domain. This had a size of $400 \times 400 \times 150\ \mu m^3$. The grid size of the computational domain was assigned small enough to ensure the grid independency of the results. The final spreading area of water on paper at four locations are shown qualitatively in Fig. 8. In order to compare modeling and experimental results, Fig. 9 shows spreading extents of a droplet in machine and perpendicular directions for modeling and experimental results. It can be observed that the spreading extends along the machine and the perpendicular directions are in the same range as those measured from the experimental results: 150–250 μm. The penetration depth in modeling cases was resulted to be 50 μm on average, which is also in good agreement with the ASA measurement results.

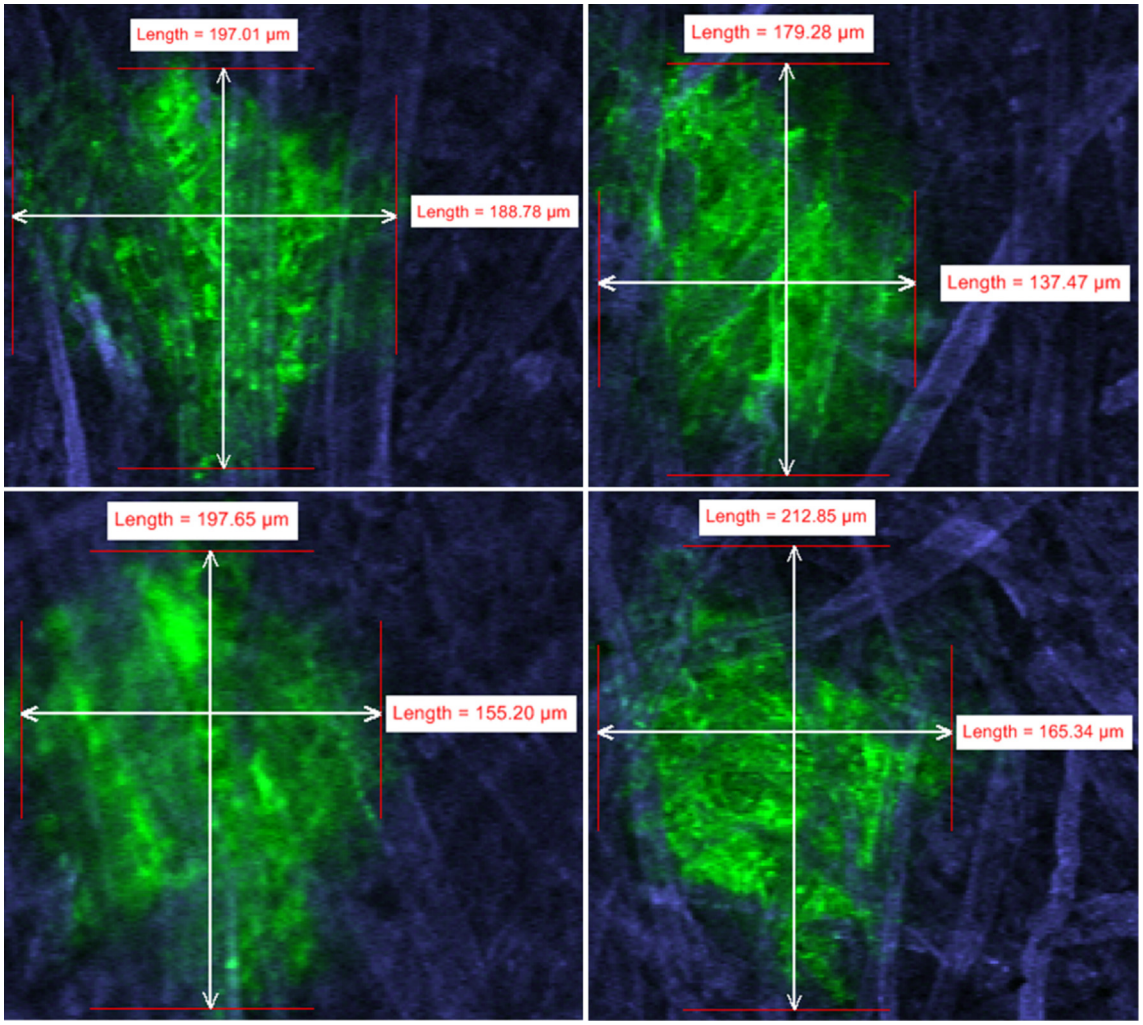

Fig. 6. Final states of liquid spread on paper at four different locations; imaging was done using confocal microscopy. Fibers are in blue and ink is seen in green.

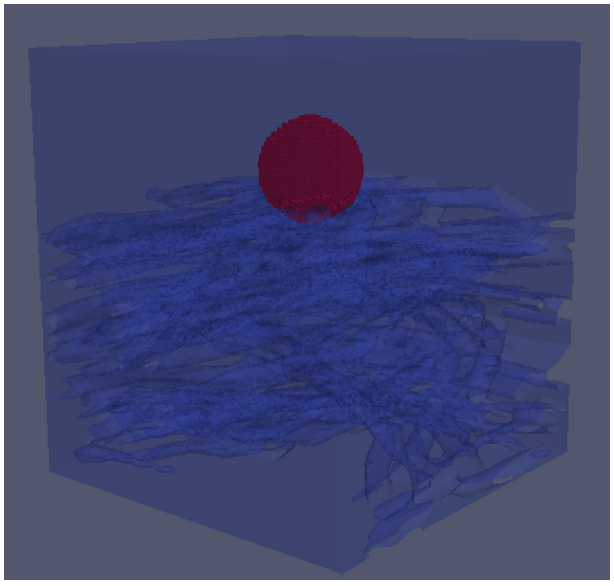

Fig. 7. Initial condition: droplet (in red color) on fibrous layer (in blue color).

3.3. Water and ink-like liquid

Simulations were also performed for a liquid with properties similar to those of ink-like liquid and results were compared with those of water. Table. 1 shows physical properties of ink-like liquid, which have been used in this study. Fig. 10 shows the distribution of the liquid phase within the fibrous layer for the case of water (10a) and ink-like liquid (10b). The extent of lateral spreading in both cases is approximately the same, but water penetrated deeper than ink-like case. Higher viscosity and lower surface tension of ink-like liquid cause less penetration depth in paper. It may be concluded that ink-like liquid, which has a higher viscosity and density, has a slower imbibition rate, as expected. The amount of water in a rectangular parallelepiped section of the domain (shown in Fig. 11) was determined and plotted over time (shown in Fig. 12). It is clear that water reaches certain depth of paper much faster than the ink-based liquid.

3.4. Contact angle effect

The hydrophilicity of surfaces, which affects the spreading and penetration depth, depends on the contact angle of the fibers and

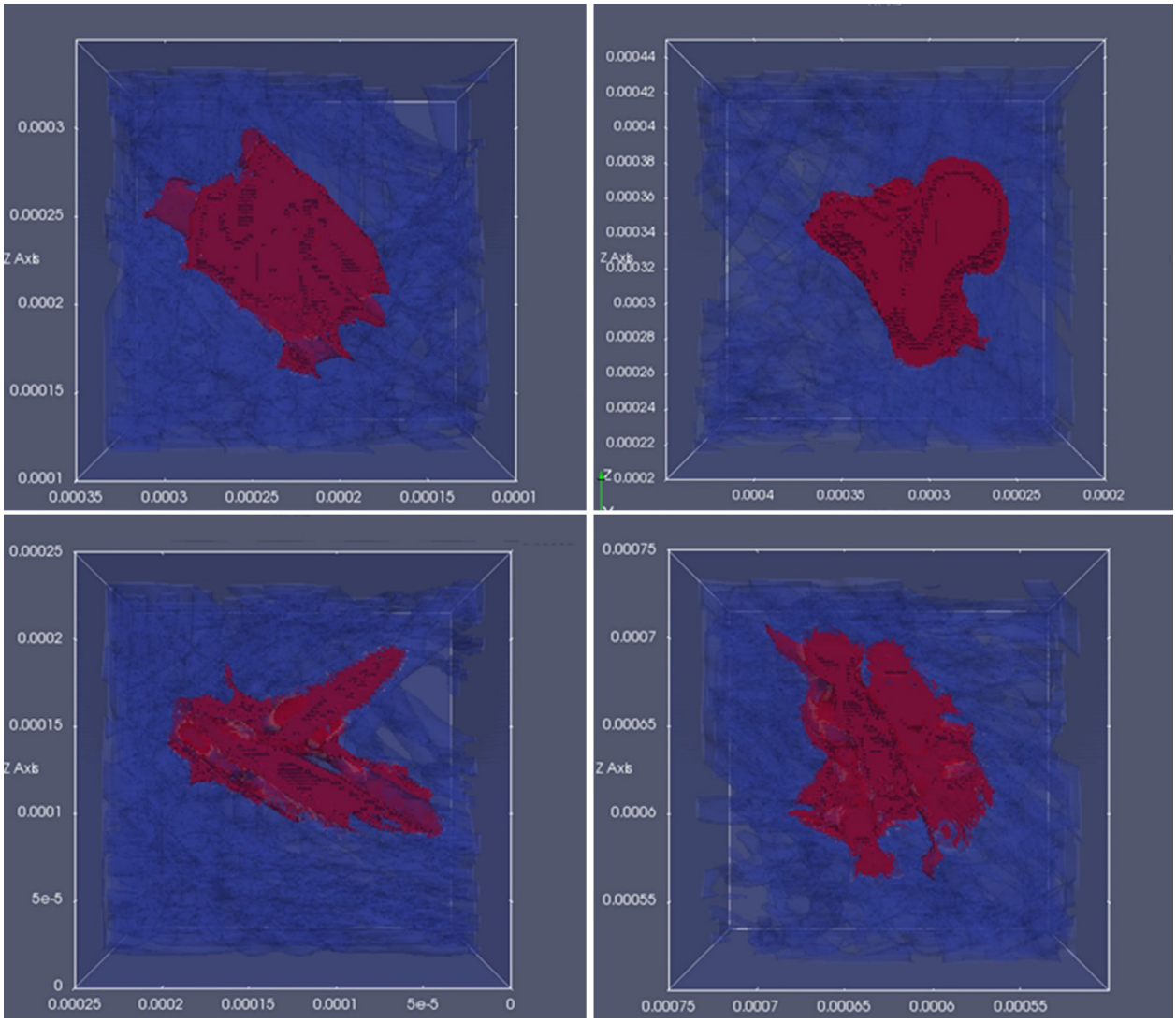

Fig. 8. Modeling results of water spreading in fibrous layer of paper at four different locations.

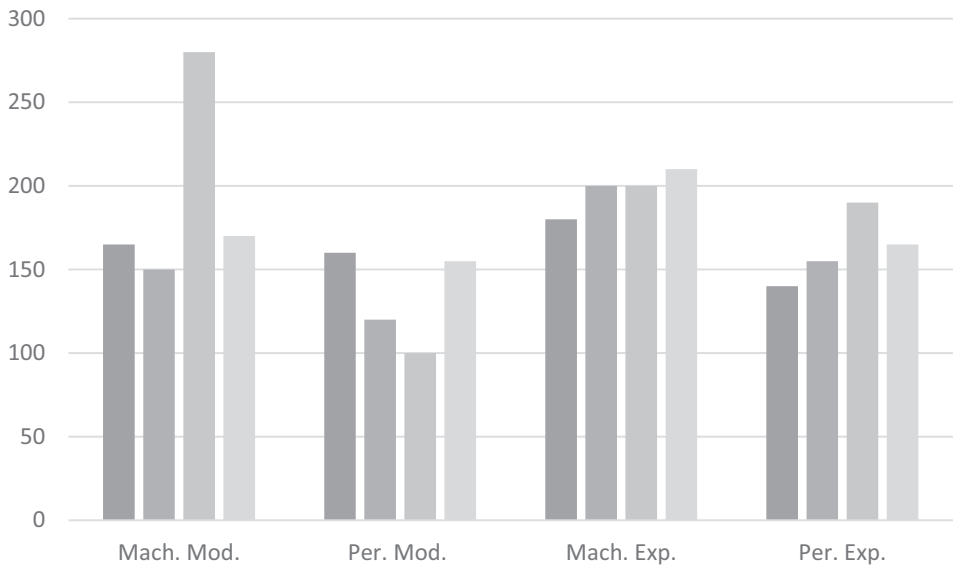

Fig. 9. Ink spreading extent in machine and perpendicular directions based on modeling and experimental results. (In × axis, Mach. and Per. are Machine and Perpendicular to machine directions respectively. Mod. and Exp. Stand for modeling and experimental results respectively.).

Table 1
Water and ink-based liquid properties.

	Kinematic viscosity (m^2/s)	Density (kg/m^3)	Surface tension (N/m)
Water	1e-6	1000	0.0707
Ink-based liquid	2e-6	2050	0.03571

liquid surface tension. While values of surface tension of water and ink-based liquid are known, to the best of our knowledge, the contact angle of an air-water meniscus on cellulose fiber surfaces is not measured yet. We did not vary the value of surface tension as its value is multiplied by cosine of contact angle. Therefore, we performed several simulations for three different contact angles of 0, 60°, and 120°. Contact angle of zero may correspond

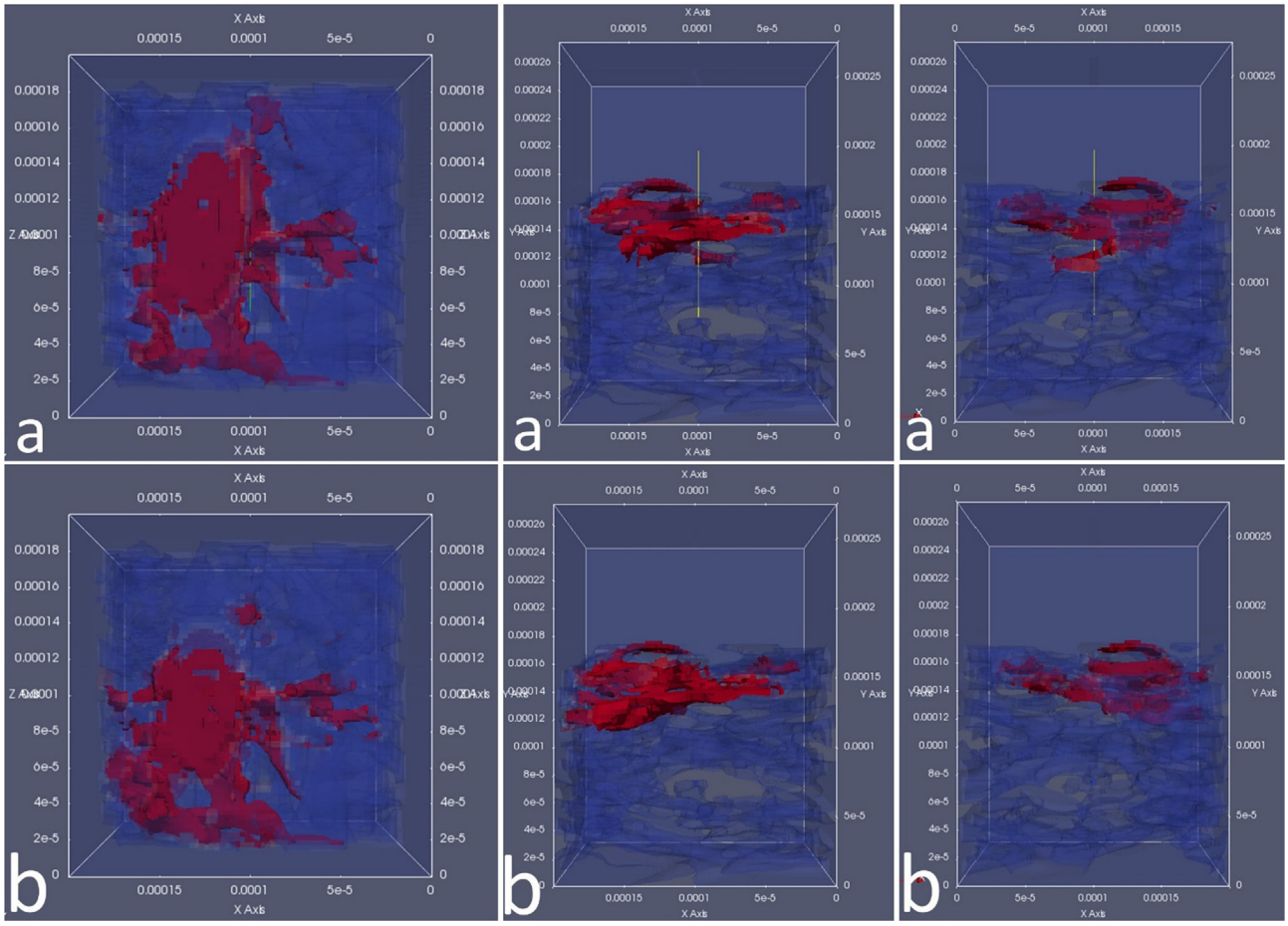

Fig. 10. Simulations results of spreading and penetration in two different cross sections; a) water and b) ink-like liquid.

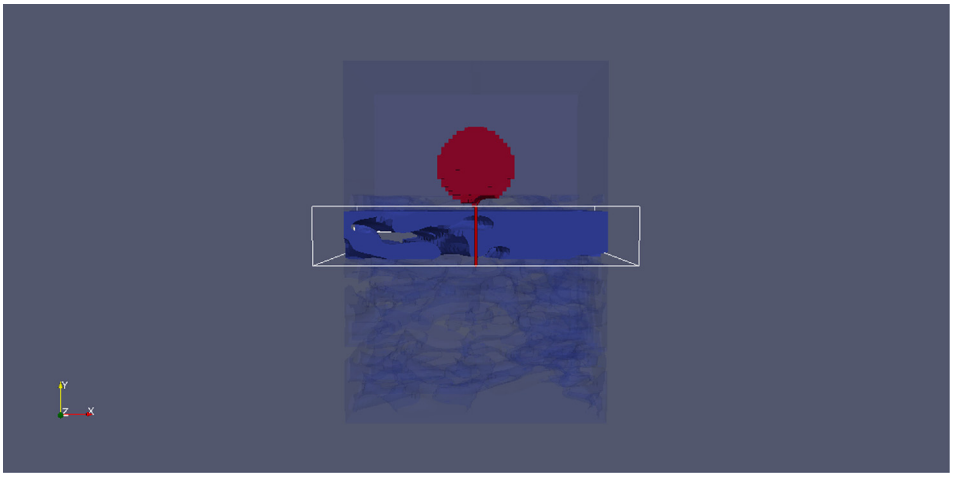

Fig. 11. Cropped domain to determine imbibition rate inside it.

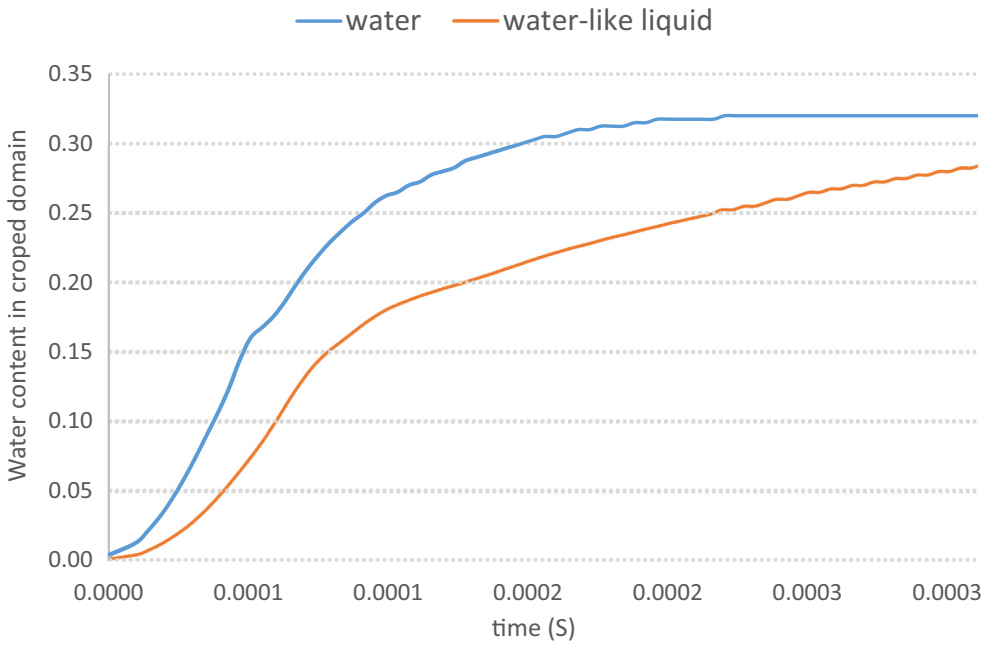

Fig. 12. Water content increase in cropped section of domain during time; for two cases, water and ink-like liquid.

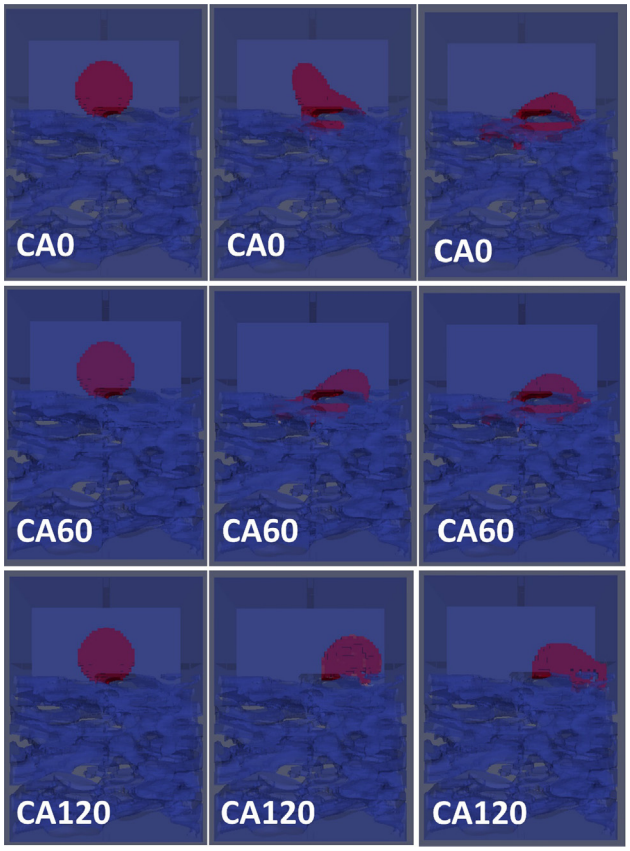

Fig. 13. Contact angle effect on water spreading/penetration in fibrous layer; a, b, and c are 0, 60°, and 120° respectively.

better to the case of water and fibers, which are primarily hydrophilic (Aslannejad et al., 2017). However, in the paper fabrication, fibers are treated to decrease their hydrophilicity. Therefore, usually larger contact angles, around 60°, may have to be considered. Fig. 13 shows the results of simulations for contact angle values of 0, 60°, and 120°. In case of contact angle of zero, we got the largest spreading and penetration depth. Increasing the hydrophobicity of the fiber surfaces, i. e. the contact angle of 60° caused less spreading and penetration depth. However, as shown in Fig. 13, the droplet moved slightly to the side (here towards the right side) before penetrating the layer. The direction of move is because of pore geometry but the contact angle is facilitating the movement. This caused movement of penetration location compared to the zero contact angle case. Therefore, this means that during printing, the ink may settle at a somewhat random location, resulting in a decrease of the print quality. In the case of contact angle of 120°, this was even more marked in the case; the droplet moved out of the domain and moved about 100 μm away from the anticipated penetration location.

The effects of contact angle on the penetration depth and spreading area are presented in Table 2. The resulting spreading/penetration lengths are in the range of values measured in experiments (the contact angle was not measured in the experiment). Penetration of water deeper into the fibrous layer may cause deformation, which is undesirable for printing. In addition, when droplet moves to sides, away from jetted location, it can cause a lower print quality. Thus, it is better to have a smaller contact angle and prevent droplet movement on fibers, and one may treat the surface so that the contact angle falls in an optimum range between 0 and 60°.

Table 2
The effect of contact angle on penetration depth and spreading area.

Contact angle	Penetration depth (μm)	Spreading area (μm^2)	Position
0	50	190 × 150	–
60	30	180 × 120	Slight droplet move to the sides
120	Not available	Not available	Dramatic droplet move to the sides

4. Conclusion

We have combined experimental and numerical studies to investigate the role of various factors on the fate of a liquid droplet deposited on an uncoated paper. The 3D structure of an uncoated paper was imaged using micro computational tomography and reconstructed to obtain a digital domain for use in numerical simulations. The spreading of a water droplet was monitored using confocal microscopy and penetration depth of water was determined based on measurements by an Automatic Scanning Absorptiometry (ASA) instrument. Simulations were performed using Volume of Fluid method. We found acceptable agreement between results of numerical simulations and experimental measurements. This provided confidence in our modelling method.

The developed model was then used to study the effect of several factors on the movement of the droplet; these were contact angle, density, viscosity, and surface tension. Simulations were performed for three different values of contact angle: 0, 60°, and 120°. Contact angle of zero showed the largest penetration depth compared to *CA*60 and *CA*120. In the case of *CA*60, the liquid moved horizontally away from the jetted location. This was even more marked in the case *CA*120. Such behavior is not desirable in printing as it can cause blurring and low quality print.

Modeling results showed that increasing the density and viscosity, all by a factor two, had insignificant effect on spreading and penetration extent. However, it took a given volume of the heavier liquid much longer to penetrate. Slower penetration means that the there is more time for the liquid to evaporate near the surface of the paper. We can postulate, therefore, that this behaviour of an ink liquid phase could be positive in that pigments and/or dye in a complete ink could be better retained near the surface.

Acknowledgements

The authors acknowledge the support received from European Research Council (ERC) under the ERC Grant Agreement No. 341225 and Océ-Technologies B.V. We also acknowledge support from the Rock and Fluids team of Shell global solution B.V. for providing us μCT images.

References

Alam, P., Toivakka, M., Backfolk, K., Sirviö, P., 2007. Impact spreading and absorption of Newtonian droplets on topographically irregular porous materials. Chem. Eng. Sci. 62, 3142–3158. https://doi.org/10.1016/j.ces.2007.03.018.

Aslannejad, H., Hassanizadeh, S.M., 2017. Study of hydraulic properties of uncoated paper: image analysis and pore-scale modeling. Transp. Porous Media. https://doi.org/10.1007/s11242-017-0909-x.

Aslannejad, H., Terzis, A., Hassanizadeh, S.M., Weigand, B., 2017. Occurrence of temperature spikes at a wetting front during spontaneous imbibition. Sci. Rep. 7, 7268. https://doi.org/10.1038/s41598-017-07528-7.

Bedram, A., Moosavi, A., 2013. Breakup of droplets in micro and nanofluidic T-junctions. J. Appl. Fluid Mech. 6, 81–86. https://doi.org/10.4028/www.scientific.net/AMM.110-116.3673.

Do-Quang, M., Carlson, A., Amberg, G., 2011. The impact of ink-jet droplets on a paper-like structure. Fluid Dyn. Mater. Process. 7, 389–402. https://doi.org/10.3970/fdmp.2011.007.389.

Fathi, H., Raoof, A., Mansouri, S.H., 2017. Insights into the role of wettability in cathode catalyst layer of proton exchange membrane fuel cell; pore scale immiscible flow and transport processes. J. Power Sources 349, 57–67. https://doi.org/10.1016/j.jpowsour.2017.03.012.

Hyväluoma, J., Raiskinmäki, P., Jäsberg, A., Koponen, A., Kataja, M., Timonen, J., 2006. Simulation of liquid penetration in paper. Phys. Rev. E 73, 036705. https://doi.org/10.1103/PhysRevE.73.036705.

Kuijpers, C.J., van Stiphout, T.A.P., Huinink, H.P., Tomozeiu, N., Erich, S.J., Adan, O.C. G., 2018. Quantitative measurements of capillary absorption in thin porous media by the Automatic Scanning Absorptometer. Chem. Eng. Sci. 178, 70–81. https://doi.org/10.1016/J.CES.2017.12.024.

Lee, H.K., Joyce, M.K., Fleming, P.D., Cameron, J.H., 2002. Production of a single coated glossy inkjet paper using conventional coating and calendering methods.

Liu, G., Fu, S., Lu, Z., Zhang, M., Ridgway, C., Gane, P., 2017. Contrasting liquid imbibition into uncoated versus pigment coated paper enables a description of imbibition into new-generation surface-filled paper. Eur. Phys. J. E 40, 111. https://doi.org/10.1140/epje/i2017-11600-y.

Modaressi, H., Garnier, G., 2002. Mechanism of wetting and absorption of water droplets on sized paper: effects of chemical and physical heterogeneity. Langmuir 18, 642–649. https://doi.org/10.1021/la0104931.

Palakurthi, N.K., Konangi, S., Ghia, U., Comer, K., 2015. Micro-scale simulation of unidirectional capillary transport of wetting liquid through 3D fibrous porous media: estimation of effective pore radii. Int. J. Multiph. Flow 77, 48–57. https://doi.org/10.1016/j.ijmultiphaseflow.2015.07.010.

Podsiadlo, P., Choi, S.-Y., Shim, B., Lee, J., Cuddihy, M., Kotov, N.A., 2005. Molecularly engineered nanocomposites: layer-by-layer assembly of cellulose nanocrystals. Biomacromolecules 6, 2914–2918. https://doi.org/10.1021/bm050333u.

Schoelkopf, J., Gane, P.A.C., Ridgway, C.J., Matthews, G.P., 2000. Influence of inertia on liquid absorption into paper coating structures. Nord. Pulp Pap. Res. J. 15, 422–430.

Weller, H.G., 2008. A New Approach to VOF-based Interface Capturing Methods for Incompressible and Compressible Flow, OpenCFD Ltd., Rep. TR/HGW/04.

Xu, L., Zhang, W.W., Nagel, S.R., 2005. Drop splashing on a dry smooth surface. Phys. Rev. Lett. 94, 184505. https://doi.org/10.1103/PhysRevLett. 94.184505.

Yarin, A.L., 2006. DROP IMPACT DYNAMICS: splashing, spreading, receding, bouncing. Annu. Rev. Fluid Mech. 38, 159–192. https://doi.org/10.1146/annurev.fluid.38.050304.092144.